ADVANCED FUNCTIONAL MATERIALS

DOI: 10.1002/adfm.200700449

A Triantennary Dendritic Galactoside-Capped Nanohybrid with a ZnS/CdSe Nanoparticle Core as a Hydrophilic, Fluorescent, Multivalent Probe for Metastatic Lung Cancer Cells**

By *Chien-Tien Chen,* Yogesh S. Munot, Santosh B. Salunke, Yi-Ching Wang,* Ruo-Kai Lin, Chun-Cheng Lin, Chia-Chun Chen,* and *Y-Hsin Liu*

A new tri-antennary, galactoside-capped gallamide dendritic anchor with thiolate focal group is synthesized via click chemistry. The highly hydrophilic dendron was efficiently anchored onto the surface of CdSe/ZnS core/shell nanoparticles in a covalent fashion, as evidenced by ^{1}H NMR spectrum of the resultant nanohybrid with intact core fluorescent property. The water-soluble nano-hybrid was found smoothly and selectively uptaken by lung cancer cells enriched with membrane-bound asialoprotein receptors in 2–3 h, as evidenced by confocal microscopic analysis. Furthermore, cancer cells that are undergoing active mitosis also tend to uptake the nanohybrids efficiently and remain sustainable in serum-containing medium for several days, which shed light on its application as a photodynamic drug carrier for apoptosis study.

1. Introduction and Background

Semiconductor nanocrystals have led to pronounced fundamental and technical interests in recent years.[1] The surface functionalized quantum dots (QDs) have shown promising applications as bioprobes, especially in cellular imaging and drug delivery, nanosensors, and LEDs.[1,2] QDs have narrow emission bandwidth, symmetrical and tunable profiles according to their size and materials composition, excellent photostability, and broad absorption spectra, making them the best choice as fluorescent probes.[3] The most common method to fabricate stable and water soluble QDs for biocompatible purpose is to chemically attach a hydrophilic organic surfactant onto the surface of nanocrystals. In recent studies, functionalization of quantum dots with biomolecules such as DNA, protein, and small biomolecules have been well established.[4]

[*] Prof. C.-T. Chen, Y. S. Munot, S. B. Salunke, Prof. C.-C. Chen, Y-H. Liu
Department of Chemistry, National Taiwan Normal University
Taipei, Taiwan; #88, Sec. 4 Ding-jou Road, Taipei 11650 (Taiwan)
E-mail: chefv043@ntnu.edu.tw

R.-K. Lin
Department of Biosciences, National Taiwan Normal University
Taipei, Taiwan; #88, Sec. 4 Ding-jou Road, Taipei 11650 (Taiwan)

Prof. Y.-C. Wang
Department of Pharmacology, College of Medicine
National Cheng Kung University (Taiwan)
E-mail: ycw5798@mail.ncku.edu.tw

C.-C. Lin
Department of Chemistry, National Tsing-Hua University
Hsin-chu (Taiwan)

[**] We thank the National Science Council of the Republic of China for a generous financial support of this research. Supporting Information is available online from Wiley InterScience or from the authors.

Glycoconjugates (e.g., glycolipids and glycoproteins) are found to play crucial roles in immune response, metastasis, fertilization, and many other bio-medicinally important processes. In particular, the research interest in glycoproteins has grown over the years due to their participating roles in cell recognition, adhesion, and growth regulation.[5] Several biological processes such as carbohydrate-protein interaction and cell-cell recognition involve multivalent interactions to achieve stronger binding as results to compensate the weak monovalent interactions. Cell surface is commonly covered with glycoconjugates, namely glycocalyx.[6a] Repulsive forces exerted by the glycocalyx can prevent nonspecific adhesion of cells.[6b] In some cell membrane configurations, however, this repulsive barrier is counterbalanced by the formation of cell-cell contacts through attractive forces. Cell-surface oligosaccharides are responsible for these specific contacts, mainly by interactions with proteins (e.g., lectins).[6b] In addition, it is evident that cells take the specific attractive forces between surface oligosaccharides as a mechanism for cell adhesion and recognition.[7] Although the existence of this interaction has been well accepted, its mechanism has not yet been clarified due to the difficulty in controlling and analyzing weak affinity interactions. Nature overcomes this problem through a polyvalent interplay between ligands and receptors at the cell surface.[8] Multivalent carbohydrate presentation with liposomes, biopolymers, and neoglycoproteins has recently been utilized for the carbohydrate-protein binding studies to obtain quantitative information of the activity enhancement relative to that from the corresponding monovalent ligands. The activity enhancement results in ''cluster effect'',[9] which trigger a series of signal transduction cascade in biological molecules.

One way to achieve the multivalent interaction in artificial system is to assemble the bioactive components onto the surface of a nanoparticle like Au or quantum dots. Glycoside-nanoparticle hybrids with differing carbohydrate monolayer density have been developed by Penadés and coworkers.[10a]

They reported the first application of glyconanoparticles as anti-adhesion tools against metastasis progression.[10b] It was found that short ex vivo pre-incubation of tumor cells with lactose coated glyconanoparticles could substantially inhibit lung cancer cell metastasis of up to 70%. We have recently utilized mannose encapsulated Au nanoparticles to label specific FimH proteins on the type 1 Pili in Escherichia coli.[11a] We subsequently demonstrated the multivalent interactions between the nanohybrids and Concanavalin A (Con A).[11b–d] Rosenzweig and co-workers have successfully, for the first time, appended carboxymethyldextran and polylysine onto succinate-modified, luminescent CdSe/ZnS QDs through electrostatic interactions, thus forming glyconanospheres.[12] The dextran residues on the nanosphere surface show high affinity toward glucose binding protein-Concanavalin A (Con A). Aoyama and co-workers have prepared water-soluble nanohybrids between carbohydrate and TOPO capped-CdSe QD by non-covalent coating of calix[4]arene-based glycocluster amphiphiles. These QD-conjugated ''sugar balls'' were utilized as endosome markers and to study endocytosis events.[13] Chaikof and co-workers used glyconanoparticles derived from the coupling of streptavidin-bound QDs with a biotin end-terminated lactose glycopolymer for the fluorescent labeling of *Ricinus communis* agglutinin-immobilized agarose beads.[14] So far, there was one report on the direct covalent attachment of one carbohydrate peripheral unit (e.g., chitosan) onto QD nanocrystals through a carboxylic focal group.[15]

2. Significance and Research Aims

Hepatocytes possess high surface density of galactose receptors. An asialoprotein is a glycoprotein treated to remove sialic acid (i.e., neuraminic acid). The resulting asialoprotein specifically binds to the galactose receptor unique to hepatocytes.[16] Galactose has been employed as a pro-drug against colon cancer and hepatoma cells due to the enrichment of galactose receptors in many cancer cell surfaces.[17a,b] Liver parenchyma cells normally have large numbers of asialoprotein receptors that strongly and specifically bind to carbohydrates containing terminal galactose residues.[17c–e] More than being an energy source, galactose-based sugar is vital for cell communication, immune response, tumor growth inhibition, enhancing wound healing, growth signals, and cell adhesion. Recent studies by Glinsky and co-workers have also shown the participating role of tumor cell Thomsen–Friedenreich (TF) disaccharide ($Gal_{\beta 1\rightarrow 3}$GalNAc-$\alpha$-OSer/Thr) sub-structures in invasion and metastasis of breast and prostate tumors.[18] In particular, their docking to microvascular endothelium is assisted by a β-galactosyl-binding protein like galectin-3. The α and β-anomers of galactosides display discernible differences in biological responses. Some specific plant-related isolectins [e.g., GS I[19] from the seeds of *Griffonia* (formerly *Bandeiraea*) *simplicifolia*] have shown stronger binding towards α-galactose than to β-galactose. On the other hand, galectins, a group of 15 β-galactoside binding lectins, are noteworthy due to their active participation in many health-related biological events.[20] More importantly, galectin-3 expression has been correlated with cancer aggressiveness,[21] metastasis,[22] and apoptosis.[23] In that context, galectin-3 is considered as an emerging cancer marker. Toward this end, mono-antennary TF glyconanoparticles with Au cores have been synthesized and their lectin affinity profiles were also examined.[24] On the other hand, di-antennary lactosidic probes with terminal groups bearing benzophenone residue at C3′-position and organic fluorescent reporter focal group have been synthesized for the detection of cancer-cell marker galectin-3.[25]

As pointed out above, quantum dot-encapsulated nanohybrids bearing peptide, protein, antibody, DNA, and other unnatural peripheral conjugates have been synthesized by using thiolates as the anchor groups and examined as fluorescent biomarkers. In marked contrast, nanohybrids possessing carbohydrate surface groups for specific cell recognition and spontaneous translocation inside the cells have never been explored.[26] So far, there was one attempt on the uses of mono-antennary maltose or Le^x-terminated long chain thiols as anchors towards CdSe quantum dots with preliminary success albeit with broad, multiple emission bands of the resultant nanohybrids presumably due to quantum-dot aggregation and in-efficient surface modification.[27] As mentioned above, there was one report associated with the use of galactose-based carbohydrates to encapsulate Au-nanoparticles in a covalent fashion. Notably, the claimed multivalent effect results only from the ensemble of the carbohydrates onto nanocrystal surface through a one-to-one peripheral-to-focal group attachment tactic. So far, the corresponding multi-antennary QD-based nanohybrids have never been explored.[28] We have recently documented the first successful synthesis of water-soluble nanohybrids (i.e., **1a** and **1b**) between gallamide-based, tri-/penta-podal dendrons and CdSe/ZnS core/shell NPs as fluorescent probes.[29] The gallamide spacer serves as a dendritic template in extending single-podal site to tri-/penta-podal site multi-antennary probes.[30] Particularly in site-to-site carbohydrate-protein interactions, moderate affinity has been identified. Wrapping such type of functionalized gallamides around nanocrystals may further enhance polyvalent interactions to biomolecules.[9b] Their preliminary biological studies indicate that the nanohybrid-**1b** derived from the penta-podal system can be effectively delivered inside Hela and lung cancer cells upon incubation for 3 h.

To understand the origin of its facile transmembrane profiles towards cancer cells and utilize the specific β-galactose recognition by cancer cells, we sought to prepare a more advanced dendritic nanohybrid-**12** with β-galactoside-encapsulated CdSe/ZnS combination and examine their trans-membrane, photodynamic profiles through Hela, kidney, and lung cancer cells in view of the enhanced cellular recognition by favorable multiple binding. Toward this probe target, thiolate was again chosen as the focal group for covalent anchoring onto the nanoparticle surface. Diethylene glycol unit was selected to bridge a spacer

ADVANCED FUNCTIONAL MATERIALS

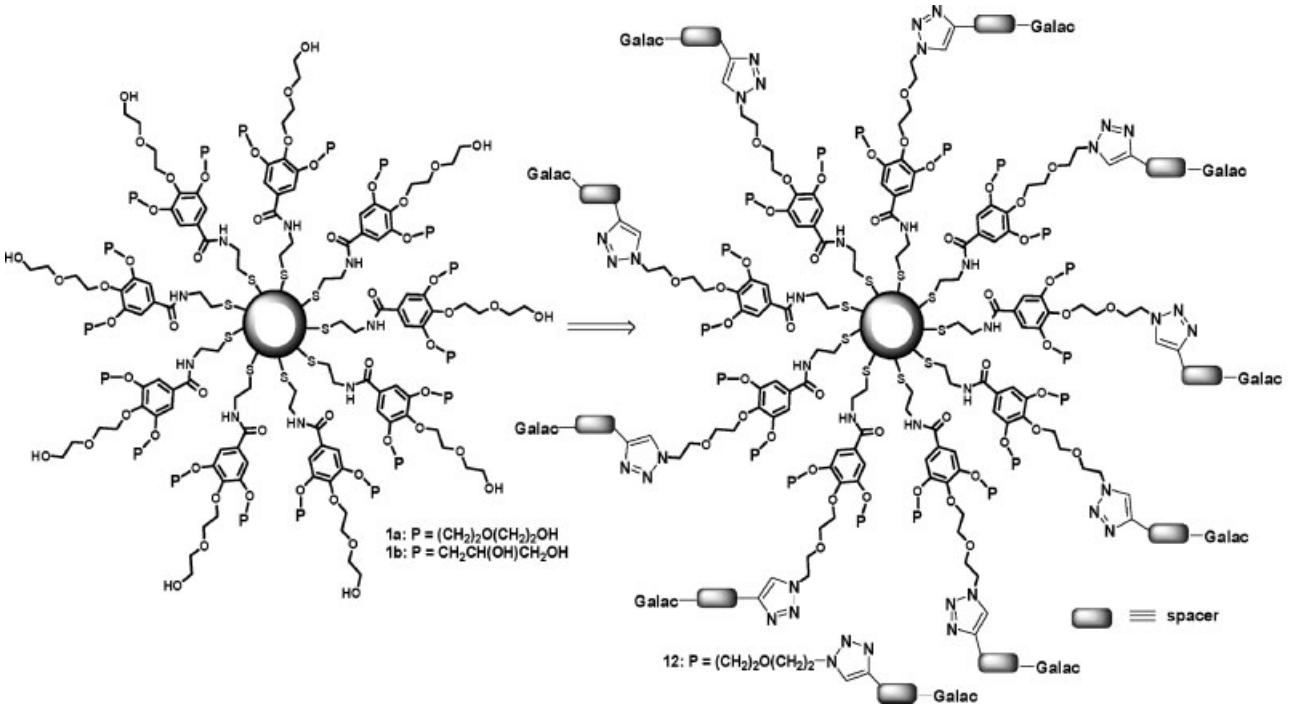

Scheme 1. Synthetic design of triantennary galactoside-capped nanohybrid **12** from the gallamide-tethered tripodal nanohybrid **1a**.

connecting the β-galactose end group in order to enhance water solubility and act as the probe for bio-receptor binding (Scheme 1).

3. Results and Discussions

To append the suitable β-glycoside unit onto the peripheral region of the dendritic, tripodal nanohybrid-**1a**, an azide–alkyne cycloaddition catalyzed by Cu(I) (i.e., click chemistry) was resorted.[31] To achieve this goal, the original tripodal dendron bearing hydroxyl terminal groups needs to be converted to the corresponding triazide dendron-**5** (Scheme 2). On the other hand, the β-galactoside-**9** has to possess a requisite propargyl unit at the glycosidic chain (Scheme 3).

The targeted tripodal, azide dendron-**5** was synthesized from methyl 3,4,5-tris-[2-(2-azido-ethoxy)-ethoxy]-benzoate-**3** (Scheme 2), which can be readily accessed from triple alkylation of methyl gallate with 2-(2-azido-ethoxy)-ethyl *p*-toluenesulfonate-**2** (3 equiv) in the presence of K_2CO_3 in refluxed CH_3CN for 24 h. The requisite azido-tosylate-**2** was prepared in two steps (92% overall yield) from 2-(chloroethoxy)ethanol by first treatment with NaN_3 in DMSO at

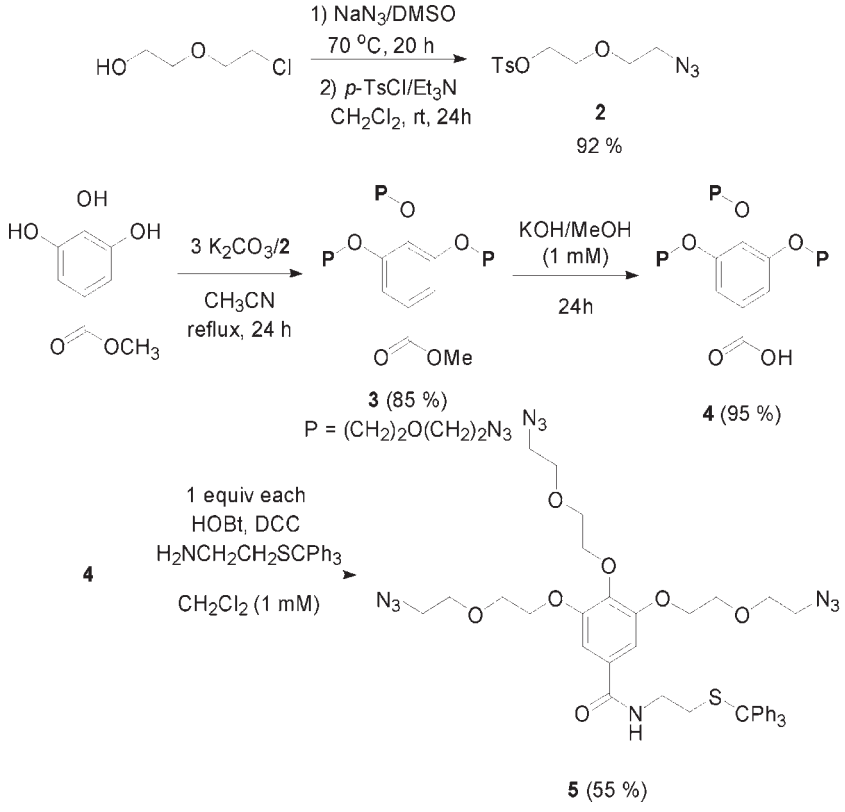

Scheme 2. Synthesis of dendritic triazide **5**.

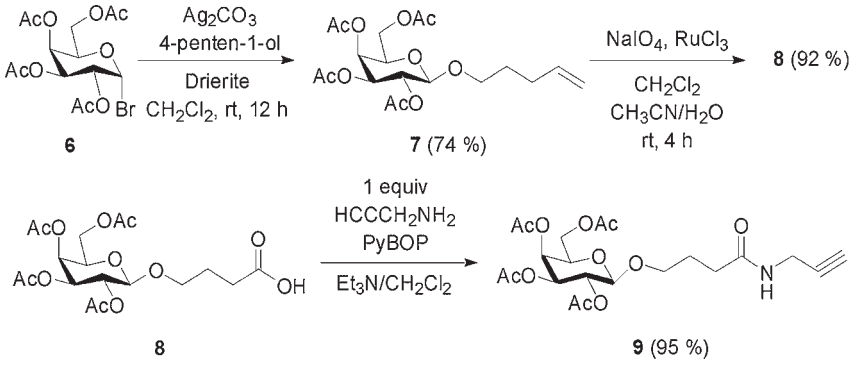

Scheme 3. Synthesis of galactosyl *N*-propargyl amide **9**.

70 °C for 18 h, followed by tosylation in a solution of Et_3N in CH_2Cl_2. The methyl ester-**3** afforded in 85% was subjected to basic hydrolysis by using KOH in warm methanol (1 mM) for 24 h to provide the corresponding acid **4** in 95% yield. Direct amidation of acid-**4** was carried out in 55% yield by coupling with 2-tritylsulfanyl-ethylamine (1 equiv) in the presence of stoichiometric dicyclohexylcarbodiimde (DCC) and 1-hydroxy benzotraizole (HOBt) in basic (Et_3N) CH_2Cl_2. The ^{1}H NMR spectrum of **5** in $CDCl_3$ shows a quartet at δ 3.27 ppm (2H) and a triplet at δ 2.51 ppm (2H), which account for the two methylene protons of $-NHCH_2CH_2SCPh_3$, respectively. In addition, the aromatic multiplets at δ 7.42– 7.18 ppm (15H) represent the triphenylmethyl protons. Furthermore, electrospray ionization (ESI) mass analysis of **5** shows a molecular ion peak at 833 ($M+Na^+$), which confirms its identity.

On the other hand, the requisite bio-probe synthon, *N*-propynyl-5-(2,3,4,6-tetra-*O*-acetyl) galactosyloxybutanamide-**9**, was prepared by modification of a reported procedure from 1-bromo-2,3,4,6-*O*-acetyl-α-D-galactopyranoside-**6** in 3 steps,[11b] Scheme 3. The displacement of the C2-bromo group in **6** by 4-penten-1-ol was performed in the presence of Ag_2CO_3 to afford 1,2-trans-selective, β-glycosylation product-**7** in 74% yield. The olefinic moiety in **7** underwent di-hydroxylation by in-situ-generated RuO_4 followed by sequential oxidative cleavage/oxidation with $NaIO_4/RuO_4$ to give acid-**8** in 92% yield. The amidation of acid-**8** with propargylamine in the presence of PyBOP as the coupling agent in basic CH_2Cl_2 gave the synthon-**9** in 95% yield.

The assembly of *N*-propargyl amide-**9** with tripodal azide dendron-**5** proceeds smoothly in the presence of catalytic $CuSO_4$ (5 mol %) and sodium ascorbate, furnishing the complete triazole-connected dendritic ligand-**10** in 95% yield, Scheme 4. The efficacy of the triple cycloaddition was further secured by NMR, DEPT, COSY, and HMQC spectroscopic analyses of **10**.[32] In particular, ^{1}H NMR spectrum of **10** reveals a singlet at δ 7.60 ppm (3H) for the triazole protons of all three branches, which shows a correlation to the triazole methine carbon at δ 123.2 ppm in ^{13}C NMR spectrum by HMQC experiment.

Furthermore, MALDI-TOF spectrometric analysis for **10** shows a molecular ion peak at 2248 ($M+Na^+$) along with two peaks corresponding to detrityl (*m/e* 2006, $M–CPh_3+Na^+$) and de-acetyl (*m/e* 2206, $M–CH_3C(O)+Na^+$) fragments, respectively, Figure 1.

Deprotection of all twelve acetyl groups in **10** was carried out in MeOH in the presence of catalytic $NaOCH_3$, leading to fully deacetylated galactoside dendron-**11a** in 95% yield. The structural identity of **11a** was confirmed by ^{1}H NMR, ^{13}C NMR, DEPT, COSY, and HMQC spectroscopic analyses. Both ^{1}H and ^{13}C NMR show the absence of any acetyl signals which were characteristic in peracetate-**10**. Furthermore, the ESI mass spectrum of **11a** shows only one parent peak at 1743.8 ($M+Na^+$) for **11a**. Final deprotection of the *S*-trityl group in **11a** by Et_3SiH in trifluoroacetic acid (TFA) led to free thiol anchor-**11b** in reasonably pure form by filtration of the reaction mixture through a short plug of Celite. Alternatively, the thiol anchor can be prepared by treatment of **10** with $V(O)OTf_2$ or MoO_2Cl_2 in refluxed EtOH with simultaneous deacetylation and de-tritylation.[33] It's ^{1}H NMR spectrum displays the presence of a triplet signal at δ 1.3 ppm as well as a quartet signal at δ 3.07 ppm responsible for the thiol and methylene protons in $-CH_2\underline{CH_2SH}$ (Figure 4a), respectively.

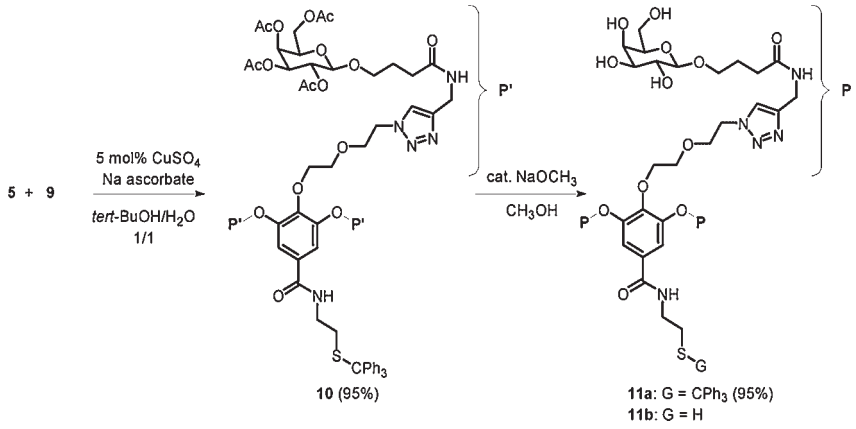

Scheme 4. Attachment of **9** to **9** through click chemistry and subsequent deacetylation-detritylation to give **11b**.

3.1. Final Nanohybrid Synthesis

The requisite CdSe/ZnS core/shell QDs for the final nanohybrid formation were prepared according to a method developed by Alivisatos and Peng.[34] Tri-*n*-octylphosphine oxide (TOPO) capped CdSe/ZnS QDs were dissolved in hexane and re-precipitated with addition of methanol to remove excess TOPO. The freshly

ADVANCED FUNCTIONAL MATERIALS

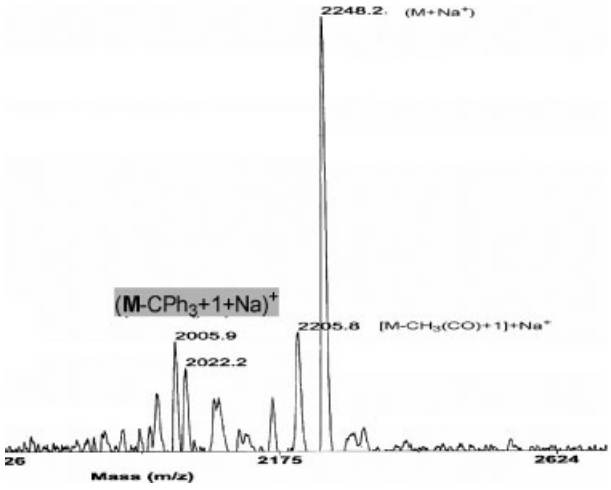

Figure 1. MALDI-TOF mass spectrum of **10**.

washed TOPO-capped CdSe/ZnS core/shell nanoparticles were heated in warm pyridine (70 °C) for 12 h and then concentrated in vacuo to give a viscous solution. The resultant pyridine-capped nanocrystals were precipitated into hexane and centrifuged. The supernatant was discarded and the precipitate was dissolved in toluene, allowing for fully replacement of TOPO by pyridine on the nanoparticle surface with preservation of their size and photoluminescence.

Pyridine was then further supplanted by ligand **11b** from the surface of CdSe/ZnS by partitioning in a biphasic system, Scheme 5. The pyridine-capped CdSe/ZnS nanocrystals were placed in toluene and a solution of the ligand **11b** in 10% aqueous MeOH with 0.5 equiv of $NaBH_4$ (to reduce the oxidized form of the thiol-**11b**) was added. The biphasic system was heated at 70–80 °C for 12–24 h to provide the desired water soluble nanohybrid-**12**. After completion of surface modification, free pyridine was removed by extensive extraction of the aqueous layer with toluene. The aqueous layer was then separated and the nanohybrid-**12** was selectively precipitated by adding THF. The pure tri-antennary, galactoside dendron-capped nanohybrid-**12** can thus be collected by centrifugation. The washing process with THF was repeated 3–4 times to remove all freely dissociated residual thiolate ligand. Notably, the direct use of TOPO-capped QDs for the same partitioning experiment led to sluggish attachment of the thiol-**11b** onto QDs as evidenced by ^{1}H NMR spectrum of the resulting nanohybrid.

The length of the tri-antennary dendron **11b** including the β-galactose terminal group, click spacer, and gallamide focal unit is about 2.8 nm. Therefore, the total diameter of the β-galactoside-conjugated nanohybrid-**12** is about (10.6 ± 0.5)-nm

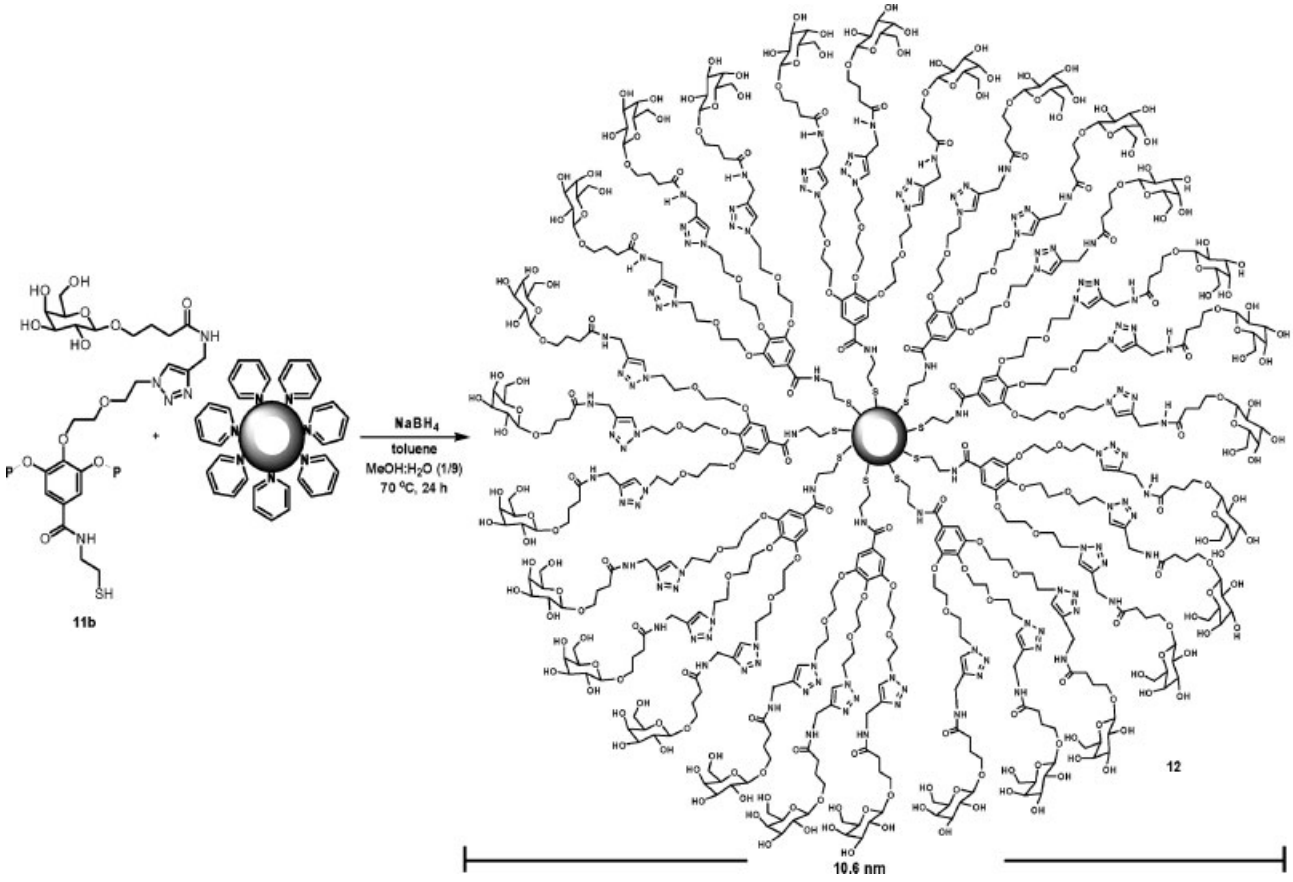

Scheme 5. Anchoring of **11b** to pyridine-capped CdSe/ZnS nanoparticles to give nanohybrid-**12.**

by using about (5 ± 0.5)-nm-sized CdSe/ZnS nanoparticles. For the characterization of the nanohybrid-**12**, its UV-VIS absorption and photoluminescence spectra (in deionized H_2O) were examined and compared with those (in toluene) of pyridine capped CdSe/ZnS core/shell nanoparticles, Figure 2. The absorption spectrum for nanohybrid-**12** shows the characteristic exciton absorption band at ca. 558 nm with 25% decrease in intensity relative to that of the original pyridine-capped nanocrystals. On the other hand, the emission maximum for **12** appears at ca. 564 nm, which is red-shifted by 8 nm as compared to that of the pyridine-capped nanocrystals presumably due to increase in the overall size of the new hybrid.

An aqueous solution of **12** in a sample vial is pale orange and transparent. After UV excitation at 355 nm of the sample vial in a dark box, the nanohybrid solution displays greenish yellow emission, Figure 3. The hybrid solution remains dispersive and homogeneous for 6 months in the refrigerator.

Further evidence in supporting the complete attachment of thiol-**11b** to the CdSe/ZnS nanoparticle surface comes from the characteristic signal changes of the -CH_2CH_2SH fragment in its

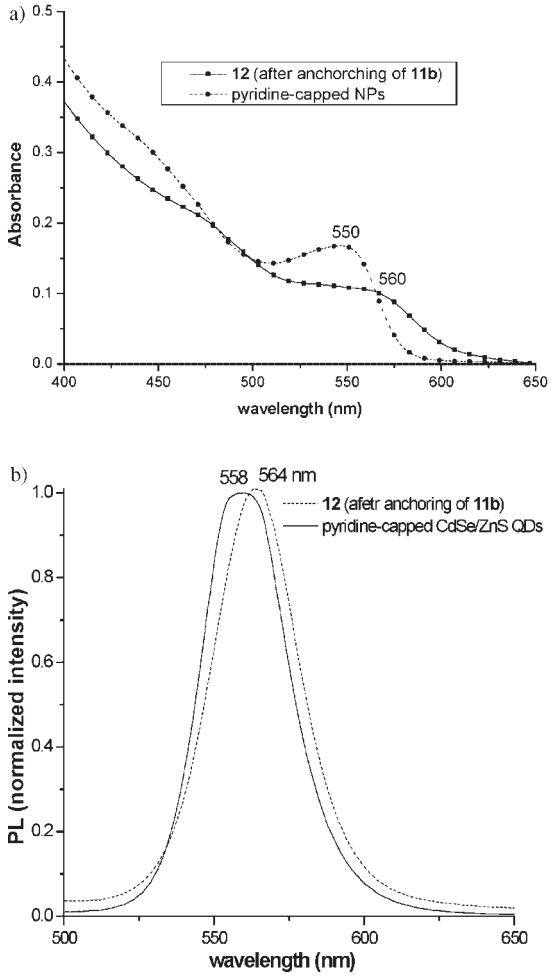

Figure 2. Absorption (top) and PL (bottom) spectra of pyridine-capped CdSe/ZnS QDs (toluene) and **12** (H_2O).

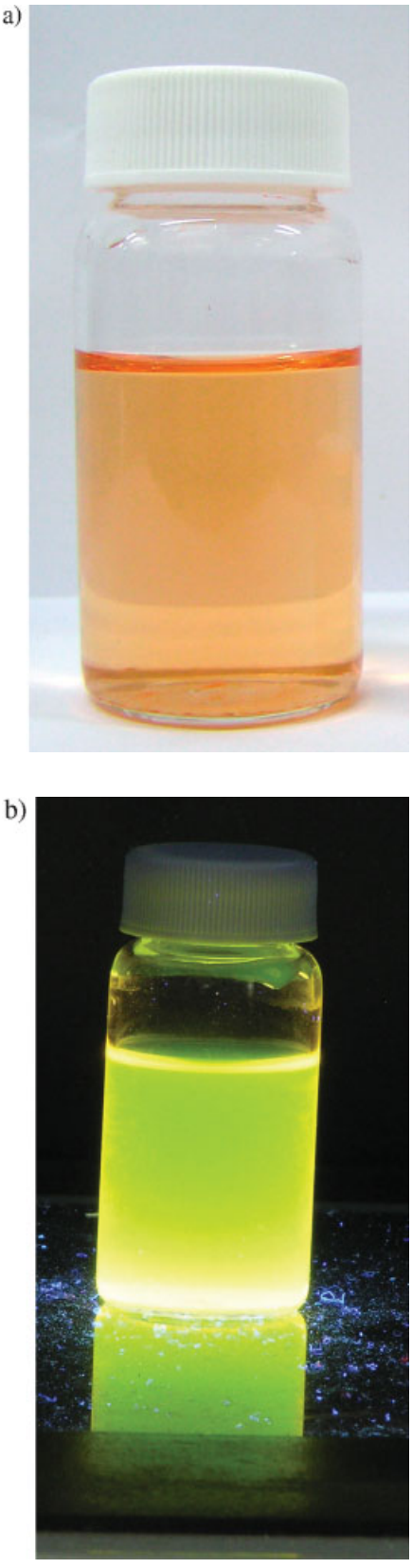

Figure 3. An aqueous solution of nanohybrid-**12** before (top) and after (bottom) UV excitation at 355 nm.

ADVANCED FUNCTIONAL MATERIALS

(in d_6-DMSO) and the corresponding nanohybrid's (in d_6-DMSO) ^{1}H NMR spectra, Figure 4. The quartet signal at δ 3.07 ppm corresponds to $-CH_2\underline{CH_2}SH$ in **11b**. Peak broadening (presumably due to hindered rotation after attachment) and slight chemical shift change (by 0.07 ppm) of the methylene unit along with disappearance of the –SH signal at δ 1.30 ppm were observed for the corresponding nanohybrid-**12**. The extent of covalent coverage by **11b** on CdSe/ZnS nanoparticle surface should be greater than 95% in view of no discernible pyridine signal and the intact integration values of the aromatic signals in the ^{1}H NMR spectrum of **12** in d_6-DMSO.

In addition, the nanoparticle size distribution for nanohybrid-**12** ranges from 4.5–5.5 nm, as determined by high resolution transmission electron microscopy (HR-TEM) measurements. The TEM images clearly indicate the uniform crystallinity of the nanocrystals in the nanohybrid, Figure 5. The highly dispersive nanohybrid **12** with narrow size distribution as evidenced by its photoluminescent and HR-TEM analyses show excellent stability for at least 6 months at ambient temperature, which poses great potential as a fluorescent, β-galactosidic nanoprobe towards the investigation of its photo-dynamic function in biosystems.

3.2. Cell Culture and Confocal Microscopy Analysis

*3.2.1. Transmembrane Profile Studies for **1b** and **12***

Human lung cancer cell line CL1-1 was obtained originally from Dr. Yang, P.C. at the Institute of Biomedical Sciences, Academia Sinica, Taiwan. A549 and H647 human lung cancer cell lines were obtained from the ATCC. CL1-1 and A549 were grown in pH 7.2 Dulbecco's Modified Eagle Medium (DMEM, from Gibco, Invitrogen corporation), containing 1% penicillin/streptomycin and 10% fetal bovine serum. And, H647 cells were grown in RPMI medium (Gibco, Invitrogen corporation) with 1% penicillin/streptomycin and 10% fetal bovine serum. Hela and COS-7 cells were obtained from the American Tissue Culture Company. All of the cells were cultured in cell culture dishes at 37 °C in humidified atmosphere with 5% CO_2 incubators.

To examine whether the pentapodal nanohybrid-**1b** and tri-antennary β-galactosidic nanohybrid-**12** can be delivered inside cancer cells upon endocytosis uptake, cancer cell incubation experiments in the presence of these nanohybrids were carried out. In a typical procedure, Hela, kidney (COS-7), or lung cancer cells were treated with 10 μM of nanohybrid **1b**

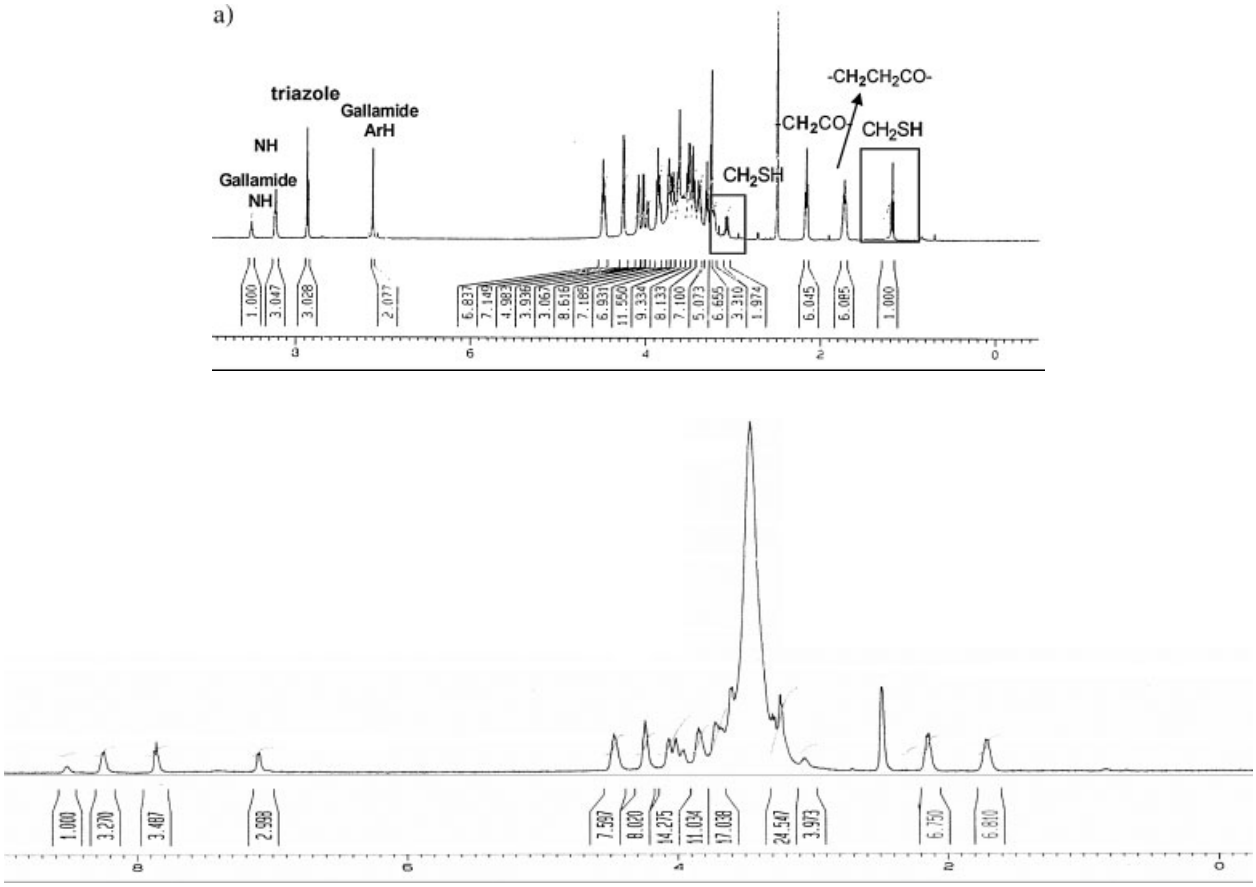

Figure 4. ^{1}H NMR spectra of free thiol **11b** (top, in d_6-DMSO) and nanohybrid-**12** (bottom, in d_6-DMSO).

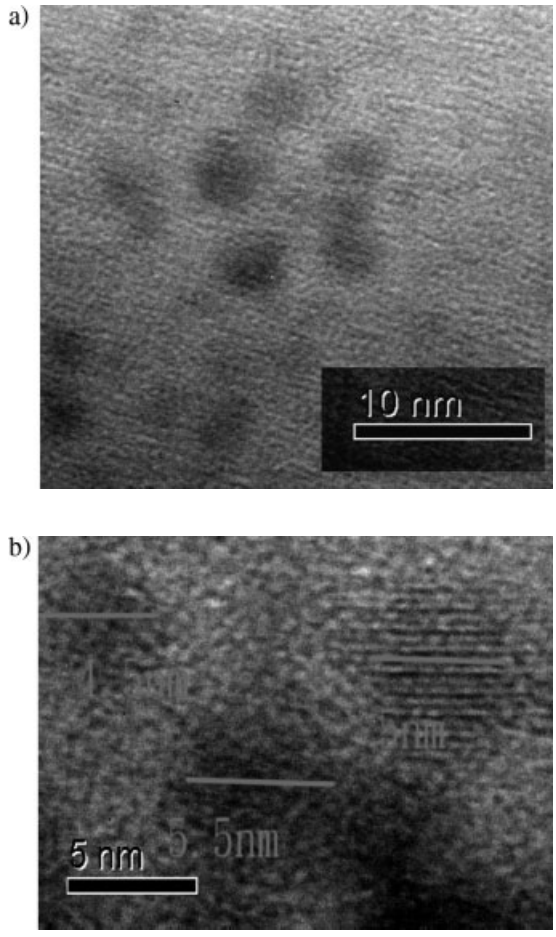

Figure 5. HR-TEM images of **12**.

or **12** for 1 h.[32] The mixture was then incubated in serum-free medium at 37 °C for 3–12 h and then washed with PBS buffer for three-times after dialysis. Hanks' Balanced Salt Solution (HBSS, Sigma–Aldrich) was used to replace the PBS during confocal observation. The images were then recorded by using Leica Microsystems TCS SP2 confocal microscope under 63× water lens with and without UV excitation. Confocal microscope images were taken with *Z*-clipping.

It was found that lung cancer cells can efficiently take up nanohybrid **1b** or **12** in 2–3 h, Figure 6 and 7. The stacked bright-field and fluorescent images allow for both cell and nanohybrid localization. The confocal microscopic image with *Z*-clipping clearly indicates that the nanohybrids enter the cancer cell cytosol rather than on the cellular surface. In addition, the endocytosis process also occurs for lung cancer cells that are undergoing mitosis. Furthermore, the nanohybrids were diffused closer to the cell-dividing nuclei. In marked contrast, negligible uptake of tripodal nanohybrid **1a** by A549 was observed under the same incubation conditions. In addition, **1a** tends to aggregate before entering A549. The results also suggest that the membrane composition for the cancer cells tend to exert stronger interaction with polyhydroxyl-ended nanohybrids **1b** and **12**, thus facilitating their faster delivery inside cancer cells. Since the transmembrane

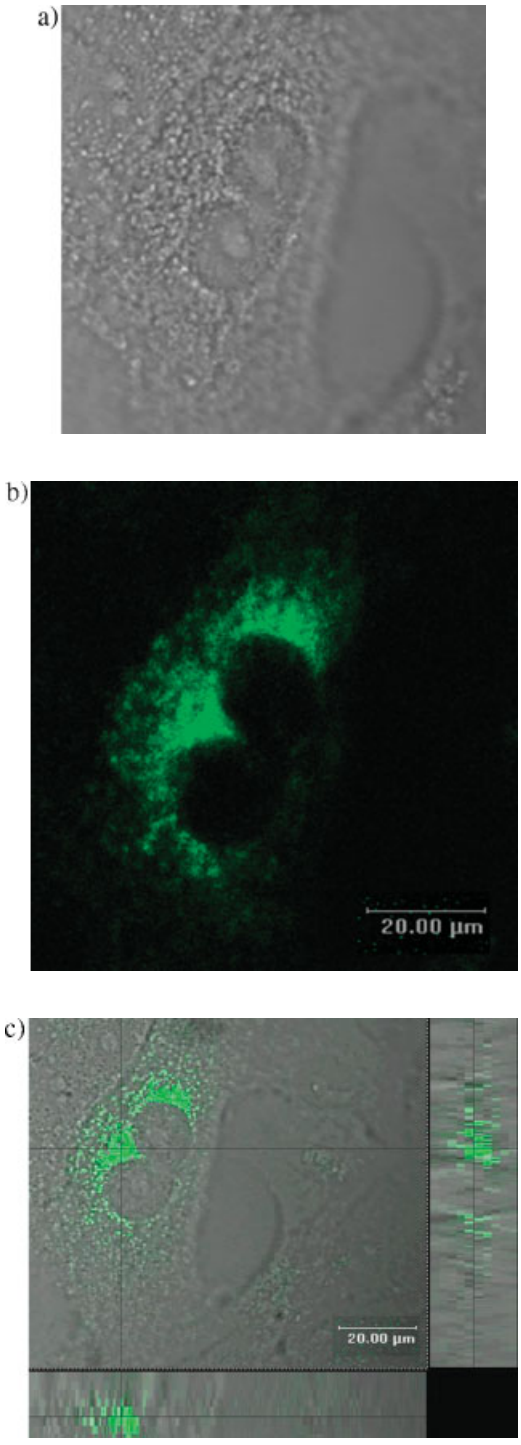

Figure 6. Images taken from incubation experiments of A549 lung cancer cells with 10 µM of pentapodal-nanohybrid-**1b** for 3 h. a) bright field image, b) fluorescence image, and c) a stacked bright-field and fluorescent image (square area) and a confocal microscopic image with Z-clipping along x and y axes.

efficiency of **1b** into A549 is somewhat slower than that exerted by **12**, the pentapodal **1b** can not fully act as a β-galactoside-mimetic of **12**.

ADVANCED FUNCTIONAL MATERIALS

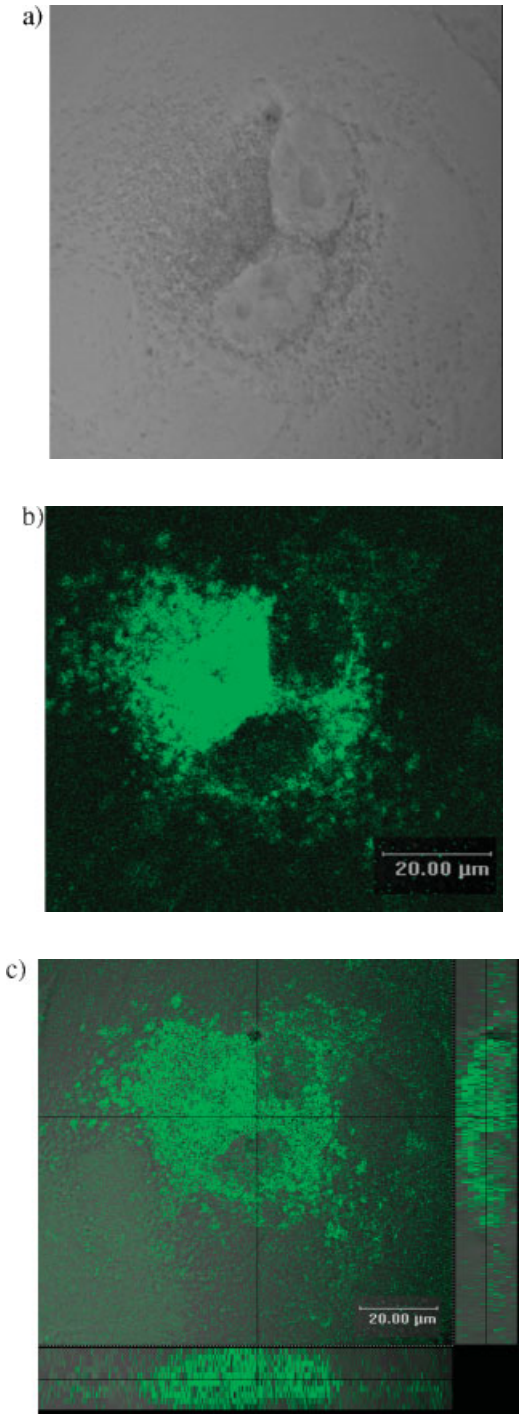

Figure 7. Images taken from incubation experiments of A549 lung cancer cells with 10 µM of tri-antennary, β-galactosidic nanohybrid-**12** for 3 h. a) bright field image, b) fluorescence image, and c) a stacked bright-field and fluorescent image (square area) and a confocal microscopic image with Z-clipping along x and y axes.

Notably, these nanohybrids tend to trigger cell aggregation upon extended incubation in buffer media. Aggregated cancer cells containing four nuclei were also detected for both cases for prolonged incubation time, Figure 8 and 9. It was found that

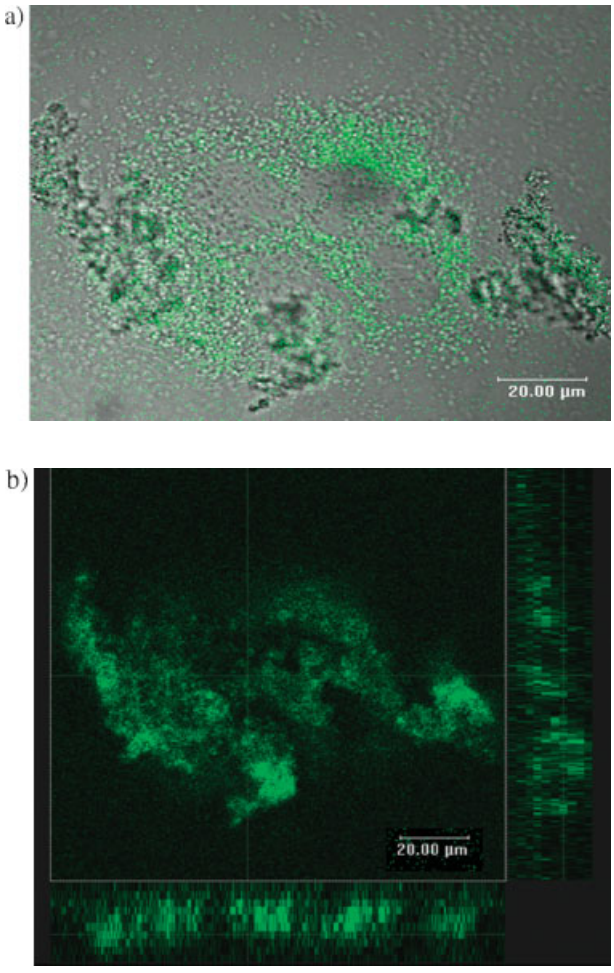

Figure 8. Images taken from incubation experiments of A549 lung cancer cells with 10 µM of pentapodal-nanohybrid-**1b** for 24 h. a) a stacked bright field and fluorescence image, b) confocal microscopic image with Z-clipping along x and y axes.

these fused cells ultimately led to cell death after 24 h. In marked contrast, the cancer cells remained alive without any aggregation for more than 48 h when they were cultured at serum-containing media in the presence of **1b** or **12**.

On the other hand, far less efficient transmembrane behaviors and no cell adhesion were observed for both Hela and kidney cancer cells upon their treatment with either **1b** or **12**, Figure 10. The nanohybrids are found much more scattered either on cell membranes or inside these cancer cells as evidenced by fluorescent microscopic images.[35] Notably, the nanohybrid-**12** remains intact with no discernible fluorescence bleaching in the endosomes over 2 days after endocytotic uptake by these cells in serum-containing medium. These observations strongly indicate that the nanohybrid-**12** is stable inside Hela and kidney cancer cells without undergoing any dissociation/decomposition at physiological pH, suggesting the low cytotoxicity of nanohybrids. Therefore, the cell death from the lung cancer cell incubation experiments with **1b** or **12** after 24 h in serum-free medium may have to do with the induced cell adhesion.

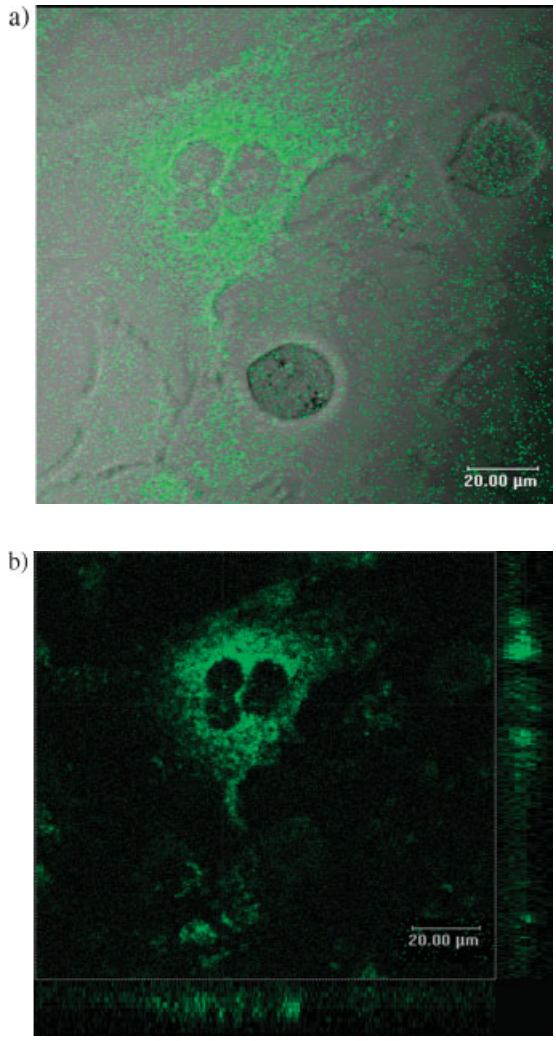

Figure 9. Images taken from incubation experiments of A549 lung cancer cells with 10 μM of tri-antennary, galactosidic nanohybrid-**12** for 24 h. a) a stacked bright field and fluorescence image, b) confocal microscopic image with Z-clipping along x and y axes.

The overall picture from the incubation experiments illustrated above indicates that the uptake of nanohybrid **1b** or **12** by A549 lung cancer cells proceeds via a receptor-mediated endocytosis. Namely, nanohybrids were first recognized by the glycoproteins on cellular surface, trapped in the endocytic vesicles, and then transferred into the endosomes of the cancer cells. The non-cytotoxic profile for nanohybrid-**12** incubated for 2–5 d in serum-containing media suggests that nanohybrid-**12** with β-galactoside peripheral units could be useful for long-term cellular fluorescent imaging.

To examine if the β-galactoside-capped, gallamide-based nanohybrid-**12** exerts any cancer cell differentiation during uptake event, we treated nanohybrid-**12** with H647 and CL1-1 lung cancer cells, respectively. Like A549 lung cancer cells, the H647 lung cancer cells are highly metastatic and enriched with β-galactose-specific asialoprotein receptors on membrane surface while the CL1-1 shows very low metastatic profile

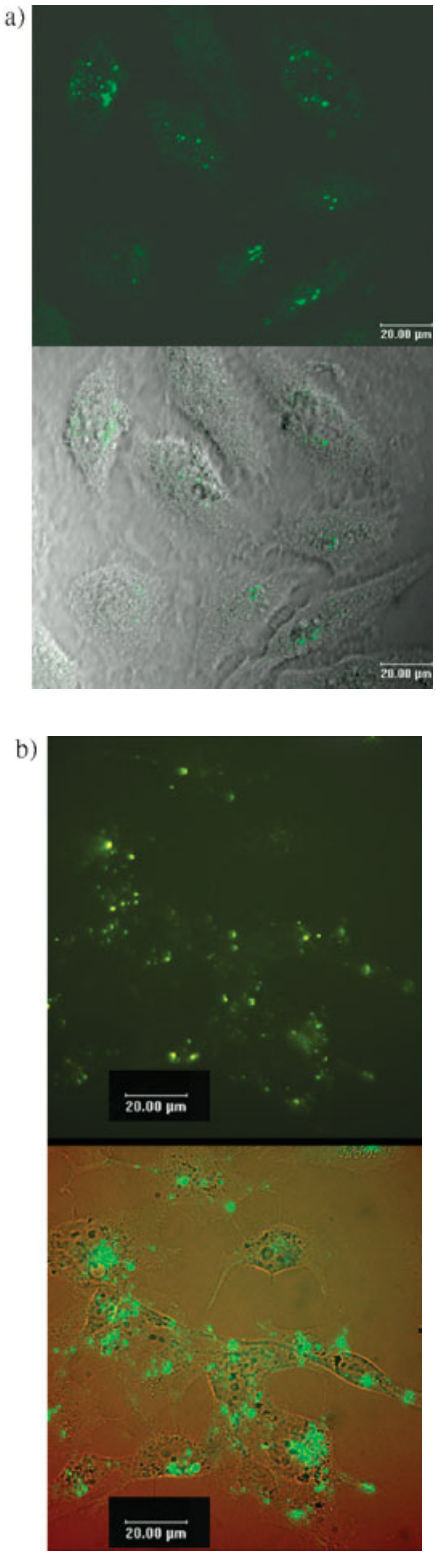

Figure 10. Images taken from incubation experiments of Hela (top) and COS-7 kidney (bottom) cancer cells with 10 μM of tri-antennary, galactosidic nanohybrid-**12** for 3 h. a) Hela: fluorescent image (top) and a stacked bright-field and fluorescent microscopic image (bottom). b) COS-7: fluorescent image (top) and a stacked bright-field and fluorescent microscopic image (bottom).

ADVANCED FUNCTIONAL MATERIALS

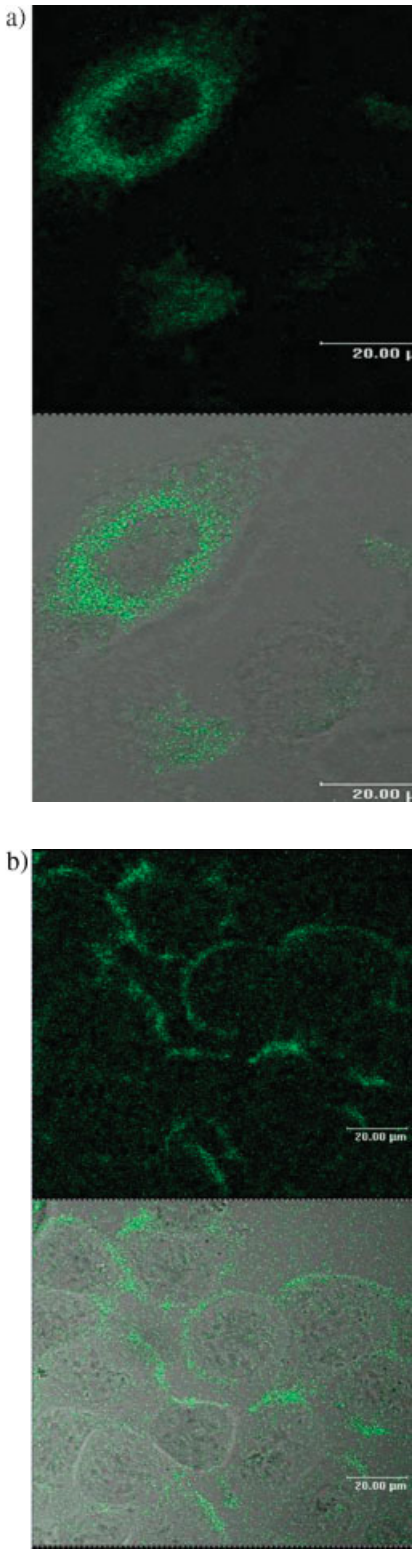

Figure 11. Images taken from incubation experiments of H647 and CL1-1 lung cancer cells with 2 μM of tri-antennary, β-galactosidic nanohybrid-**12** for 2–3 h. a) H647: fluorescent (top) and a stacked bright-field and fluorescent (bottom) microscopic images, b) CL1-1: fluorescent (top) and a stacked bright-field and fluorescent (bottom) microscopic images.

with very low expression of asialoprotein receptors on its surface. It was found that nanohybrid-**12** was efficiently delivered inside H647 cancer cells in 3 h, Figure 11. On the contrary, all the nanohybrids remained on the cellular surface under the same incubation conditions in the case of CL1-1. The results further support that the translocation of nanohybrid-**12** inside A549 and H647 lung cancer cells was indeed through receptor-mediated endocytosis. Therefore, nanohybrid-**12** may serve as a useful drug carrier with cancer cell differentiation, allowing for photodynamic tracing studies.

4. Conclusion

We have developed a new tri-antennary, β-galactoside-capped gallamide dendron synthesis. A click methodology was employed to achieve the facile assembly of the dendron with a thiolate focal group, which can secure CdSe/ZnS core/shell nanoparticle in the center by covalent anchoring as evidenced by ^{1}H NMR spectrum of the resultant nano-hybrid with intact core fluorescent property.

We have demonstrated another successful example of using biphasic extraction system for efficient dative/covalent ligand exchange on the surface of CdSe/ZnS nanocrystals. The resultant nanohybrid becomes highly water soluble with intact morphology of the nanocrystal core. The nanohybrid-**12** can be smoothly delivered inside Hela, kidney, and metastatic lung cancer cells with differential rates as evidenced by confocal microscopic analyses. The transmembrane efficiency is increased with increasing density profile of asialoprotein receptors on cellular surface, indicating a receptor-mediated endocytosis. A control CL1-1 lung cancer cell with low-expression of asialoprotein receptors on membrane surface blocks the translocation of nanohybri-**12** into cell endosomes. Furthermore, lung cancer cells that are undergoing active mitosis also tend to uptake the nanohybrids efficiently and remain sustainable in serum-containing media for several days, which shed light on its potential application as a photodynamic drug carrier for apoptosis studies. The newly designed tri-antennary multivalent nanoprobe-**12** is potentially useful for studying the multimeric carbohydrate interactions, understanding endocytic process as well cell adhesion and recognition. Therefore, the galactosidic nanohydrid and its carbohydrate derivatives may serve as a convenient photodynamic tool to monitor cell-cell adhesion and recognition processes where carbohydrates are intensively involved.

5. Experimental

General: ^{1}H NMR and ^{13}C NMR spectra were recorded on Jeol JVM-EX400 (400 MHz ^{1}H, 100 MHz ^{13}C) spectrometers in deuterochloroform with chloroform as an internal reference unless otherwise stated. Chemical shifts are reported in ppm (δ). Coupling constants, *J*, are reported in Hz. Infrared spectra were recorded on a Perkin-Elmer Paragon-500 FTIR spectrometer. Peaks are reported in units of cm^{-1} with the following relative intensities: br (broad), s (strong 67–100%), m (medium 33–67%), or w (weak 0–33%). Mass spectra

were recorded on a Finnigan TCQ-700 spectrometer with an ionization voltage of 70 or 20 eV unless otherwise stated. Elemental analyses were obtained on a Heraeus CHN-OS Rapid analyzer or by the Northern Instrument Center of Taiwan. Fast atom bombardment (FAB) mass spectra were recorded on a Finnigan MAT-95S spectrometer. Electrospray ionization (ESI) mass spectra were recorded on a Thermo Finnigan spectrometer equipped with LCQ Advantage ionization and Spectra System detector systems. Data are reported in the form *m*/*e* (intensity relative to base peak). Analytical TLC was performed on Merck silica gel plates with QF-254 indicator. Visualization was accomplished with UV light or with phosphomolybdic acid (PMA) and $KMnO_4$ staining agents. Column (flash) chromatography was performed using 32–63 μm silica gel. Optical rotations were recorded on a JASCO DIP-1000 digital polarimeter and are reported as follows: $[\alpha]^T$ (c = g/100 mL, solvent). THF and toluene were dried over benzophenone-ketyl intermediate under nitrogen atmosphere and distilled before use. MeOH was dried over magnesium turnings under nitrogen atmosphere and distilled before use. All reaction products were isolated as chromatographically pure materials. The experimental procedures and analytical data for **1a** and **1b** have been reported previously [29].

Transmission Electron Microscopy (TEM) Experiments: The average sizes, size distribution and crystallinity of the nanohybrid sample-**12** were confirmed by a JEOL-2010F transmission electron microscopy operated at 200 KV. Samples for TEM measurements were prepared by depositing an aliquot of the water-soluble nanohybrid solution in toluene onto either an amorphous carbon film or a porous carbon film on a Cu grid.

*Methyl 3,4,5-Tris-[2-(2-azido-ethoxy)-ethoxy]-benzoate (**3**)*: A mixture of methyl gallate (1.84 g, 10 mmol), K_2CO_3 (4.55 g, 33 mmol), and 2-(2-azido-ethoxy)-ethyl *p*-toluenesulfonate **2** (9.4 g, 33 mmol, 1.1 equiv) in CH_3CN (100 mL) was refluxed for 24 h. After completion of the reaction as monitored by TLC, the reaction mixture was cooled to ambient temperature and then filtered by washing with $CHCl_3$ (3 × 10 mL). The combined organic filtrates were evaporated to dryness. The crude residue was purified by column chromatography on silica gel (EtOAc/*n*-hexane 3/7) to give 4.83 g (93%) of **3** as yellow syrup: ^{1}H NMR (400 MHz, $CDCl_3$, δ): 7.30 (s, 2H), 4.23 (t, J = 4.6 Hz, 2H, CH_2), 4.20 (t, J = 4.7 Hz, 4H, 2 × CH_2), 3.88–3.85 (m, 7H, 2 × CH_2, OCH_3), 3.81 (t, J = 4.8 Hz, 2H, CH_2), 3.74–3.71 (m, 6H, 3 × CH_2), 3.40–3.35 (m, 6H, 3 × CH_2); ^{13}C NMR (100 MHz, $CDCl_3$, δ): 166.4, 152.1, 142.4, 125.1, 109.0, 72.3, 70.6, 70.1, 69.8, 69.6, 68.8, 52,1, 50.8, 50.7; MS (ESI) calcd for $C_{20}H_{29}N_9O_8$: 523.50, found: 547 ($M + Na^+$, 100%); High Resolution-MS calcd for $C_{20}H_{29}N_9O_8$: 523. 2139, found: 523.2108; R_f 0.30 (EtOAc/*n*-hexane, 3/7).

*3,4,5-Tris-[2-(2-azido-ethoxy)-ethoxy]-benzoic Acid (**4**)*: A solution of methyl 3,4,5-tris-[2-(2-azido-ethoxy)-ethoxy]-benzoate **3** (514 mg, 1 mmol) and powdered KOH (130 mg, 2.25 mmol) in methanol (30 mL) was refluxed for 12 h. After having been cooled to ambient temperature, the reaction mixture was concentrated. The residue was acidified with 1 N HCl (15 mL) to pH 1 at 0 °C and the whole mixture was extracted with EtOAc (3 × 15 mL). The combined organic layers were washed with water (10 mL), brine (5 mL), dried ($MgSO_4$), and evaporated. The crude residue was purified by column chromatography on silica gel (EtOAc/*n*-hexane 1/1) to give 484 mg (95%) of **4** as yellow syrup: ^{1}H NMR (400 MHz, $CDCl_3$, δ): 7.38 (s, 2H), 4.28 (d, J = 4.6, 2H), 4.24–4.21 (m, 4H), 3.90–3.88 (m, 6H), 3.88–3.42 (m, 6H), 3.42–3.38 (m, 6H); ^{13}C NMR (100 MHz, $CDCl_3$, δ): 171.2, 151.8, 143.2, 124.2, 109.6, 72.4, 70.7, 70.2, 70.1, 69.9, 69.74, 69.6, 68.9, 68.3, 50.81, 50.78, 50.6; MS (ESI) calcd for $C_{19}H_{27}N_9O_8$: 509.47, found: 532 ($M + Na^+$, 100%); High Resolution-MS calcd for $C_{19}H_{27}N_9O_8$: 509.1983, found: 509.1908; R_f 0.25 (EtOAc/*n*-hexane, 1/1).

*N-[(2-Trimethylmethylsulfanyl)ethyl]-3,4,5-tris-[2-(2-azido-ethoxy)-ethoxy]-benzamide (**5**)*: To a solution of 2-tritylsulfanyl-ethylamine (319 mg, 1 mmol) and Et_3N (101 mg, 1 mmol) in CH_2Cl_2 (15 mL) was added 1-hydroxybenzotriazole (HOBT, 135 mg, 1 mmol) at 0 °C. A solution of *N*,*N*′-dicyclohexylcarbodiimide (DCC, 206 mg, 1 mmol) and 3,4,5-tris-[2-(2-azido-ethoxy)-ethoxy]-benzoic acid **4** (509 mg, 1 mmol) in CH_2Cl_2 (30 mL) was slowly added. The resulting reaction mixture was gradually warmed to ambient temperature and stirred for 12 h. After completion of the reaction as monitored by TLC, the reaction mixture was filtered and the filtrate was evaporated. The residue re-dissolved in EtOAc (15 mL) was washed with saturated aqueous $NaHCO_3$ (5 mL), water (5 mL), dried ($MgSO_4$), and evaporated. The crude residue was purified by column chromatography (EtOAc/*n*-hexane, 7/3) on silica gel to give 445 mg (55%) amide **5** as white solid: ^{1}H NMR (400 MHz, $CDCl_3$, δ): 7.42–7.40 (m, 6H, aromatics Hs), 7.29–7.26 (m, 6H, aromatics Hs), 7.24–7.18 (m, 3H, aromatic Hs), 7.01 (s, 2H), 6.28 (bt, J = 5.7 Hz, 1H, NH), 4.24–4.19 (m, 6H, 3 × CH_2), 3.86–3.82 (m, 6H, 3 × CH_2), 3.75–3.69 (m, 6H, 3 × CH_2), 3.40–3.37 (m, 6H, 3 × CH_2), 3.27 (q, J = 6.2 Hz, 2H, NHCH_2), 2.51 (t, J = 6.4 Hz, 2H, CH_2SCPh$_3$); ^{13}C NMR (100 MHz, $CDCl_3$, δ): 166.6, 152.4, 144.6, 141.5, 129.7, 129.4, 127.9, 126.7, 107.3, 72.3, 70.6, 70.1, 69.8, 69.7, 69.2, 66.8, 50.8, 50.7, 38.7, 32.0; MS (ESI) calcd for $C_{40}H_{46}N_{10}O_7S$: 810.92, found: 833.0 ($M + Na^+$, 100%); R_f 0.25 (EtOAc/*n*-hexane, 7/3).

(1-Pentenyl)-2,3,4,6-tetra-O-acetyl-β-D-galactopyranoside (**7**) [11b]: To a stirred suspension of Drierite (2.0 g), Ag_2CO_3 (2.0 g), and 4-penten-1-ol (1.0 mL, 9.78 mmol) in anhydrous CH_2Cl_2 (20 mL) was slowly added a solution of 1-bromo-2,3,4,6-tetra-*O*-acetyl-*β*-D-galactopyranoside[11a] (2.0 g, 4.86 mmol) in anhydrous CH_2Cl_2 (15 mL) at ambient temperature. The reaction mixture was stirred overnight and then filtered through a short plug of (3 cm OD, 2–3 cm high) of Celite. The Celite cake was washed with CH_2Cl_2 (2 × 15 mL). The combined organic filtrates were washed with water (10 mL), brine (10 mL), dried ($MgSO_4$), and evaporated. The crude residue was purified by column chromatography on silica gel (EtOAc/hexane, 1/2) to afford 1.58 g (74%) of the *β*-anomer **7** as a colorless oil: ^{1}H NMR (400 MHz, $CDCl_3$, δ): 5.82–5.72 (m, 1H), 5.37 (d, J = 3.2 Hz, 1H), 5.19 (dd, J = 10.5, 7.9 Hz, 1H), 5.02–4.95 (m, 3H), 4.44 (d, J = 7.9 Hz, 1H), 4.19–4.08 (m, 2H), 3.91–3.86 (m, 2H), 3.51–3.45 (m, 1H), 2.15, 2.04, 2.03, and 1.97 (s, 12H, 4 × OC(O)CH_3), 2.13–2.06 (m, 2H), 1.73–1.58 (m, 2H); ^{13}C NMR (100 MHz, $CDCl_3$, δ): 170.4, 170.3, 170.2, 169.3, 137.8, 115.0, 101.3, 70.9, 70.6, 69.3, 68.9, 67.1, 61.3, 29.8, 28.6, 20.9, 20.7, 20.6, 20.6; High Resolution-MS (FAB) calcd for $C_{19}H_{29}O_{10}$ (M + H): 417.1761, found: 417.1764.

*4-(3,4,5-Triacetoxy-6-acetoxymethyl-tetrahydropyran-2-yloxy)-butanoic Acid (**8**)*[36]: $RuCl_3$-H_2O (151 mg, 0.72 mmol) and $NaIO_4$ (3.12 g, 14.60 mmol, 4 equiv) were added to a vigorously stirred solution of **7** (1.52 g, 3.65 mmol) in aqueous CH_2Cl_2/CH_3CN (1/1, 20 mL in 15 mL H_2O). After having been stirred at ambient temperature for 2 h, the reaction mixture was treated with an additional amount of $NaIO_4$ (1.56 g, 2 equiv) and then stirred for 2 more h. The reaction mixture was diluted with water (10 mL) and then extracted with CH_2Cl_2 (3 × 20 mL). The combined organic extracts were dried ($MgSO_4$), filtered, and evaporated. The crude residue was purified by column chromatography on silica gel (EtOAc) to give 1.48 g (92%) of acid **8** as a colorless oil: ^{1}H NMR (400 MHz, $CDCl_3$, δ): 5.38 (d, J = 3.3 Hz, 1H), 5.19 (dd, J = 10.5, 8.0 Hz, 1H), 5.01 (dd, J = 10.5, 3.4 Hz, 1H), 4.45 (d, J = 7.9 Hz, 1H), 4.22–4.07 (m, 2H), 3.97–3.93 (m, 1H), 3.89 (t, J = 6.8 Hz, 1H), 3.58–3.53 (m, 1H), 2.44 (t, J = 7.2 Hz, 2H), 2.15, 2.06, 2.04, 1.98 (s, 12H, 4 × OC(O)CH_3), 1.94–1.88 (m, 2H); ^{13}C NMR (100 MHz, $CDCl_3$, δ): 177.5, 170.5, 170.3, 170.2, 169.6, 101.3, 70.9, 70.7, 68.8, 68.6, 67.0, 61.3, 30.0, 24.5, 20.7, 20.6, 20.6, 20.6; High Resolution-MS (FAB) calcd for $C_{18}H_{27}O_{12}$ (M + H): 435.1503, found: 435.1508.

*N-2-Propynyl-4-(3,4,5-triacetoxy-6-acetoxymethyl-tetrahydropyran-2-yloxy)-butanamide (**9**)*: A solution of acid **8** (435 mg, 1 mmol) in anhydrous CH_2Cl_2 (7 mL) was added BOP (435 mg, 1 mmol) and Et_3N (101 mg, 1 mmol) at ambient temperature. The resulting solution was stirred for 0.5 h and then treated with propargyl amine (58 mg, 1.05 mmol) and Et_3N (101 mg, 1 mmol). The resulting reaction mixture was stirred for 24 h and then quenched with 1N HCl (5 mL). The aqueous layer was separated and extracted with CH_2Cl_2 (3 × 10 mL). The combined organic extracts were washed with brine (5 mL), dried ($MgSO_4$), and evaporated. The crude residue was purified by column chromatography on silica gel (EtOAc/*n*-hexane, 7/3) to give 447 mg (95%) amide **9** as a colorless oil: ^{1}H NMR (400 MHz, $CDCl_3$, δ):

5.86 (bs, 1H), 5.39 (dd, $J = 3.3$, 0.8 Hz, 1H), 5.18 (dd, $J = 10.5$, 7.9 Hz, 1H), 5.01 (dd, $J = 10.5$, 3.4 Hz, 1H), 4.46 (d, $J = 7.9$ Hz, 1H), 4.20–4.10 (m, 2H), 4.05–4.03 (m, 2H), 3.92–3.85 (m, 2H), 3.62–3.58 (m, 1H), 2.29–2.25 (m, 2H), 2.23 (t, $J = 2.5$ Hz, 1H), 2.15 (s, 3H), 2.07 (s, 3H), 2.05 (s, 3H), 1.98 (s, 3H), 1.94–1.89 (m, 2H); ^{13}C NMR (100 MHz, $CDCl_3$, δ): 172.3, 170.4, 170.2, 170.1, 169.6, 101.3, 79.5, 71.5, 70.8, 70.7, 68.9, 67.9, 67.0, 61.2, 32.3, 29.1, 25.4, 20.8, 20.62, 20.61, 20.5; MS (ESI) calcd for $C_{21}H_{29}NO_{11}$: 471.46; found: 494.0 ($M + Na^+$, 100%); High Resolution-MS calcd for $C_{21}H_{29}NO_{11}$: 471.1741, found: 471.1734; TLC R_f 0.30 (EtOAc/*n*-hexane, 7/3).

*Click Triazide-5 and N-2-Propynyl-galactosylated Amide-9 to Get Dendron-***10**: *N*-(2-tritylsulfanyl-ethyl)-3,4,5-tris-[2-(2-azido-ethoxy)-ethoxy]-benzamide **5** (810 mg, 1 mmol) and *N*-2-propynyl-4-(3,4,5-triacetoxy-6-acetoxymethyl-tetrahydropyran-2-yloxy)-butanamide **9** (1413 mg, 3 mmol, 1 equiv) were suspended in a 1:1 mixture of water and *tert*-butanol (100 mL). Aqueous sodium ascorbate (1 mL, 1 M, 1 mmol) was added to the above mixture followed by addition of aqueous $CuSO_4 \cdot 5H_2O$ (0.15 mmol, in 1 mL of water). The resulting heterogeneous mixture was stirred vigorously and became clear at the end of the reaction. The reaction mixture was concentrated and then diluted with water (50 mL). The whole mixture was extracted with CH_2Cl_2 (3×30 mL). The combined organic extracts were dried ($MgSO_4$), filtered, and evaporated. The crude residue was passed through a short silica gel column (4 cm OD, 4 cm high; MeOH/CH_2Cl_2, 30/70) to give 2472 mg (94%) of peracetylated galactosyl gallamide **10** as white solid: ^{1}H NMR (500 MHz, $CDCl_3$, δ): 7.60 (s, 3H, $3 \times$ triazole H), 7.35 (d, $J = 7.4$ Hz, 6H), 7.29–7.22 (m, 6H), 7.19–7.16 (m, 3H), 7.03 (s, 2H), 6.79 (bt, $J = 5.6$ Hz, 1H, NH), 6.74 (bt, $J = 5.6$ Hz, 2H, NH), 5.36 (d, $J = 3.2$ Hz, 3H), 5.28 (s, 2H), 5.15–5.11 (m, 3H), 5.01–4.98 (m, 3H), 4.46–4.35 (m, 16H), 4.15–4.07 (m, 9H), 4.02 (t, $J = 3.3$ Hz, 2H), 3.90–3.79 (m, 11H), 3.74 (t, $J = 4.2$ Hz, 3H), 3.65 (t, $J = 4.3$ Hz, 2H), 3.55–3.49 (m, 3H), 3.31 (q, $J = 6.3$ Hz, 2H, CH_2NH), 2.51 (t, $J = 6.5$ Hz, 2H, CH_2SCPh$_3$), 2.23–2.17 (m, 6H, $3 \times CH_2$), 2.13–2.11 (m, 9H), 2.01 (s, 18H), 1.96 (s, 9H), 1.88–1.81 (m, 6H, $3 \times CH_2$); ^{13}C NMR (125 MHz, $CDCl_3$, δ): 172.6, 170.3, 170.2, 170.0, 169.5, 166.8, 152.1, 144.6, 140.9, 130.0, 129.5, 127.9, 127.8, 126.7, 123.2, 107.4, 101.2, 72.1, 70.8, 70.61, 70.57, 69.7, 69.4, 69.13, 69.07, 69.02, 68.9, 68.8, 67.0, 66.7, 61.2, 53.4, 50.2, 39.0, 34.8, 32.3, 32.0, 25.4, 20.7, 20.6, 20.6, 20.5; MALDI-TOF MS calcd for $C_{103}H_{133}N_{13}O_{40}S$: 2225.2, found: 2248.2 ($M + Na^+$, 100%); TLC R_f 0.30 (MeOH/CH_2Cl_2, 30/70).

*3,4,5-Tris-[2-[2-(4-{[4-(3,4,5-trihydroxy-6-hydroxymethyl-tetrahydro-pyran-2-yloxy)-butyrylamino]-methyl}-[1,2,3]triazol-1-yl)-ethoxy]-ethoxy}-N-(2-tritylsulfanyl-ethyl)-benzamide (***11a***)*: A solution of the gallactoside dendrimer **10** (0.250g, 0.1 mmol) in MeOH (7 mL) was treated with NaOMe (10 mg). The reaction mixture was stirred at ambient temperature for 12 h. To the crude reaction mixture was added acidic Sephadex resin (50×) and the whole mixture was filtered through a short plug of silica gel to get 0.178 g (96%) of pure deacetylated dendrimer **11a** as a colorless liquid: ^{1}H NMR (500 MHz, DMSO-d_6, δ): 8.51 (t, $J = 5.5$ Hz, 1H, NH), 8.23 (t, $J = 5.5$ Hz, 3H, NH), 7.88 (s, 2H, triazole H), 7.86 (s, 1H, triazole H), 7.35–7.29 (m, 12H), 7.26–7.22 (m, 3H), 7.13 (s, 2H), 4.50–4.46 (m, 6H) 4.26 (d, $J = 5.5$ Hz, 6H), 4.08 (t, $J = 3.8$ Hz, 3H), 4.03 (t, $J = 9.7$ Hz, 3H), 3.98 (t, $J = 4.6$ Hz, 3H), 3.87–3.83 (m, 6 H), 3.75–3.72 (m, 6H), 3.71–3.68 (m, 7H), 3.54–3.50 (m, 7 H), 3.48–3.44 (m, 8H), 3.41–3.36 (m, 7H), 3.31–3.29 (m, 4H), 3.26–3.20 (m, 3H), 3.10–3.04 (m, 2H), 2.31 (t, $J = 7.1$ Hz, 2H, CH_2S), 2.16 (t, $J = 7.4$ Hz, 6H, $3 \times CH_2$, CH_2CO), 1.73 (quin, $J = 7.2$ Hz, 6H, $3 \times CH_2$, CH_2CH_2CO); ^{13}C NMR (125 MHz, DMSO-d_6, δ): 171.9, 165.3, 151.6, 144.8, 144.8, 144.4, 139.8, 129.0, 128.0, 126.7, 123.0, 106.3, 103.4, 75.1, 73.4, 70.6, 68.9, 68.7, 68.2, 68.1, 68.0, 65.9, 60.4, 49.31, 49.26, 45.6, 34.1, 31.8, 31.3, 25.5; MS (ESI) calcd for $C_{79}H_{109}N_{13}O_{28}S$: 1720.8, found: 1743.8 ($M + Na^+$, 100%); TLC R_f 0.30 (MeOH/CH_2Cl_2, 85/15).

*Nanohybrid (***12***)*: A mixture of **11a** (86 mg, 0.05 mmol) in trifluoroacetic acid (TFA, 5 mL) was treated with Et_3SiH (0.05 mL) at ambient temperature. White precipitate was formed instantly and was removed by filtration through a short plug of Celite. The filtrate was concentrated to give crude thiol-**11b** which was identified by ^{1}H NMR and was used directly for the next anchoring step. A solution of pyridine-capped CdSe/ZnS core/shell nanocrystals (15 mg) in toluene (5 mL) was mixed with stirring with a solution of free thiol-**11b** and $NaBH_4$ (0.05 equiv) in 50% aqueous MeOH (7 mL) at 70 °C for 24 h. The reaction mixture was cooled. The aqueous layer was separated and extracted with toluene (5×7 mL) to give the crude nanohybrid solution. The nanohybrid **12** was purified by induced precipitation of the aqueous layer with THF and then collected by centrifugation. For ^{1}H NMR analysis of the pure-**12**, DMSO-d_6 was added to the centrifuged residue-**12** and the solution was set under high vacuum in the dark for 5 min to remove any residual solvents (like THF, toluene, and MeOH) used for the reaction. The ^{1}H NMR spectrum for **12** in DMSO-d_6 shows the average extent of coverage on CdSe/ZnS nanoparticles by **11b** (free thiolate) to be at least above 95% with discernible pyridine ligand (Figure 4).

Received: April 19, 2007
Revised: July 3, 2007

[1] a) A. P. Alivisatos, *Science* **1996**, *271*, 933. b) W. C. Chen, S. Nie, *Science* **1998**, *281*, 2016. c) G. Markovich, C. P. Collier, S. E. Henrichs, F. Remacle, R. D. Levine, J. R. Heath, *Acc. Chem. Res.* **1999**, *32*, 415. d) L. Brus, *J. Phys. Chem.* **1986**, *90*, 2555.

[2] a) A. P. Alivisatos, *Nature* **1994**, *370*, 354. b) A. A. Mamedov, A. Belov, M. Giersig, N. N. Mamedova, N. A. Kotov, *J. Am. Chem. Soc.* **2001**, *123*, 7738. c) See also: W. J. Parak, R. Boudreau, M. Le Gros, D. Gerion, D. Zanchet, C. M. Micheel, S. C. Williams, A. P. Alivisatos, C. Larabell, *Adv. Mater.* **2002**, *14*, 882.

[3] a) C. B. Murray, D. J. Norris, M. G. Bawendi, *J. Am. Chem. Soc.* **1993**, *115*, 8706. b) M. Bruchez, M. Moronne, P. Gin, S. Weiss, A. P. Alivisatos, *Science* **1998**, *281*, 2013. c) H. Mattousi, J. M. Mauro, E. R. Goldmann, G. P. Anderson, V. C. Sundar, F. V. Mikulec, M. G. Bawendi, *J. Am. Chem. Soc.* **2000**, *122*, 12142. d) A. P. Alivisatos, *Pure Appl. Chem.* **2000**, *72*, 3. e) A. J. Sutherland, *Curr. Opin. Solid State Mater. Sci.* **2002**, *6*, 365.

[4] a) X. Michalet, F. F. Pinaud, L. A. Bentolila, J. M. Tsay, S. Doose, J. J. Li, G. Sundaresan, A. M. Wu, S. S. Gambhir, S. Weiss, *Science* **2005**, *307*, 538. b) W. J. Parak, T. Pellegrino, C. Plank, *Nanotechnology* **2005**, *16*, R9. c) G. P. Mitchell, C. A. Mirkin, R. L. Letsinger, *J. Am. Chem. Soc.* **1999**, *121*, 8122. d) Y. A. Wang, J. J. Li, H. Chen, X. Peng, *J. Am. Chem. Soc.* **2002**, *124*, 2293. e) X. Gao, L. Yang, J. A. Petros, F. F. Marshall, J. W. Simons, S. Nie, *Curr. Opin. Biotechnol.* **2005**, *16*, 63.

[5] a) Y. Lee, R. Lee, *Acc. Chem. Res.* **1995**, *28*, 321. b) R. A. Dwek, *Chem. Rev.* **1996**, *96*, 683.

[6] a) A. Frey, K. T. Giannasca, R. Weltzin, P. J. Giannasca, H. Reggio, W. I. Lencer, M. R. Neutra, *J. Exp. Med.* **1996**, *184*, 1045. b) A. Varki, *Glycobiology* **1993**, *3*, 97.

[7] a) K. M. Koeller, C.-H. Wang, *Chem. Rev.* **2000**, *100*, 4465. b) S.-I. Hakomori, *Pure Appl. Chem.* **1991**, *63*, 473.

[8] J. J. Lundquist, E. J. Toone, *Chem. Rev.* **2002**, *102*, 555.

[9] a) Y. Lee, R. R. Townsend, M. R. Hardy, J. Lonngren, J. Arnap, M. Haraldsson, H. J. Lonn, *J. Biol. Chem.* **1983**, *258*, 199. b) M. Mammen, S. K. Choi, G. M. Whitesides, *Angew. Chem. Int. Ed.* **1998**, *37*, 2754.

[10] a) A. G. Barrientos, J. M. de la Fuente, T. C. Rojas, A. Fernandez, S. Penadés, *Chem. Eur. J.* **2003**, *9*, 1908. b) J. Rojo, V. Diaz, J. Fuente, I. Segura, A. G. Barrientos, H. H. Riese, A. Bernad, S. Penadés, *Chem. Bio. Chem.* **2004**, *5*, 291.

[11] a) C. C. Lin, Y.-C. Yah, C.-Y. Yang, C.-L. Chen, G.-F. Chen, C.-C. Chen, Y.-C. Wu, *J. Am. Chem. Soc.* **2002**, *124*, 3508. b) C. C. Lin, Y. C. Yeh, C. Y. Yang, G. F. Chen, Y. C. Chen, Y. C. Wu, C. C. Chen, *Chem. Commun.* **2003**, 2920. For reviews, see: c) H. Lis, N. Sharon, *Chem.*

Rev. **1998**, *98*, 637. d) R. Shenhar, V. M. Rotello, *Acc. Chem. Res.* **2003**, *36*, 549.

[12] Y. Chen, T. Ji, Z. Rosenzweig, *Nano Lett.* **2003**, *3*, 581.

[13] F. Osaki, T. Kanamori, S. Sando, T. Sera, Y. Aoyama, *J. Am. Chem. Soc.* **2004**, *126*, 6520.

[14] X.-L. Sun, W. Cui, C. Haller, E. L. Chaikof, *Chem. Bio. Chem.* **2004**, *5*, 1593.

[15] M. Xie, H.-H. Liu, P. Chen, Z.-L. Zhang, X.-H. Wang, Z.-X. Xie, Y.-M. Du, B.-Q. Pan, D. W. Pang, *Chem. Commun.* **2005**, 5518.

[16] D. A. Wall, G. Wilson, A. L. Hubbard, *Cell* **1980**, *21*, 79.

[17] a) G. Ashwell, A. G. Morell, *Adv. Enzymol. Relat. Areas Mol. Biol.* **1974**, *41*, 99. b) Y. Ohya, H. Oue, K. Nagatomi, T. Ouchi, *Biomacromolecules* **2001**, *2*, 927. c) M. Spiess, *Biochemistry* **1990**, *29*, 10009. d) R. T. Lee, P. Lin, Y. C. Lee, *Biochemistry* **1984**, *23*, 4255. e) F. J. Feher, K. D. Wyndham, D. J. Knauer, *Chem. Commun.* **1998**, 2394.

[18] V. V. Glinsky, G. V. Glinsky, K. Rittenhouse-Olson, M. E. Huflejt, O. V. Glinskii, S. L. Deutcher, T. P. Quinn, *Cancer Res.* **2001**, *61*, 4851.

[19] a) J. Lescar, R. Loris, E. Mitchell, C. Gautier, V. Chazalet, V. Cox, L. Wyns, S. Pérez, C. Breton, A. Imberty, *J. Biol. Chem.* **2002**, *277*, 6608. b) M. Schwarz,1 L. Spector, A. Gargir, A. Shtevi, M. Gortler, R. T. Altstock, A. A. Dukler, N. Dotan, *Glycobiology* **2003**, *13*, 749.

[20] a) H. Leffler, S. Carlsson, M. Hedlund, Y. Qian, F. Poirier, *Glycoconjugate J.* **2002**, *19*, 433. b) R. J. Pieters, *Chem. Bio. Chem.* **2006**, *7*, 721.

[21] S. Califice, V. Castronovo, F. van den Brûle, *Int. J. Oncol.* **2004**, *25*, 983.

[22] Y. Takenaka, T. Fukumori, A. Raz, *Glycoconjugate J.* **2002**, *19*, 543.

[23] a) S. Nakahara, N. Oka, A. Raz, *Apoptosis* **2005**, *10*, 267. b) F.-T. Liu, G. A. Rabinovich, *Nat. Rev. Cancer* **2005**, *5*, 29.

[24] S. A. Svarovsky, Z. Azekely, J. J. Barchi, Jr., *Tetrahedron: Asymmetry* **2005**, *16*, 587.

[25] L. Ballell, M. van Scherpenzeel, K. Buchalova, R. M. J. Liskamp, R. J. Pieters, *Org. Biomol. Chem.* **2006**, *4*, 4387.

[26] a) J. M. de la Fuente, S. Penadés, *Biochim. Biophys. Acta* **2006**, *1760*, 636. b) J. M. de la Fuente, S. Penadés, *Glycoconjugate J.* **2004**, *21*, 149.

[27] a) J. M. de la Fuente, S. Penadés, *Tetrahedron: Asymmetry* **2005**, *16*, 387. b) See also: A. Robinson, J.-M. Fang, P. T. Chou, K. W. Liao, R. M. Chu, S.-J. Lee, *Chem. Bio. Chem.* **2005**, *6*, 1899.

[28] a) Tri-antennary glyco-silicas with peripheral α-mannoside have been prepared [28b] but their structural identities were not confirmed and their affinity strengths towards ConA was found to be less efficient than that from the original unfunctionalized silica. b) M. Ortega-Muñoz, J. Lopez-Jaramillo, H. Hernandez-Mateo, F. Santoyo-Gonzalez, *Adv. Synth. Catal.* **2006**, *348*, 2410.

[29] C.-T. Chen, V. D. Pawar, Y. S. Munot, C.-C. Chen, C.-J. Hsu, *Chem. Commun.* **2005**, 2483.

[30] Y. A. Wang, J. J. Li, J. Chen, X. Peng, *J. Am. Chem. Soc.* **2002**, *124*, 2293.

[31] a) Z. P. Demko, K. B. Sharpless, *Angew. Chem. Int. Ed.* **2002**, *41*, 2113. b) For a recent application in mannose-capped dendrimer synthesis, see: P. Wu, M. Malkoch, J. N. Hunt, R. Vestberg, E. Kaltgrad, M. G. Finn, V. V. Fokin, K. B. Sharpless, C. J. Hawker, *Chem. Commun.* **2005**, *46*, 5775.

[32] See the Supporting Information for details.

[33] a) C.-T. Chen, J.-H. Kuo, C.-H. Li, N. B. Barhate, S.-W. Hon, T.-W. Li, S.-D. Chao, C.-C. Liu, Y.-C. Li, I.-H. Chang, J.-S. Lin, C.-J. Lin, Y.-C. Chou, *Org. Lett.* **2001**, *3*, 3729. b) C.-T. Chen, J.-H. Kuo, C.-H. Ku, S.-S. Weng, C.-Y. Liu, *J. Org. Chem.* **2005**, *70*, 1328. c) C.-T. Chen, S.-S. Weng, J.-Q. Kao, C.-C. Lin, M.-D. Jan, *Org. Lett.* **2005**, *7*, 3343. d) S.-S. Weng, Y.-D. Lin, C.-T. Chen, *Org. Lett.* **2006**, *8*, 5633.

[34] a) X. G. Peng, M. C. Schlamp, A. V. Kadavanich, A. P. Alivisatos, *J. Am. Chem. Soc.* **1997**, *119*, 7019. b) Z. A. Peng, X. G. Peng, *J. Am. Chem. Soc.* **2001**, *123*, 183.

[35] Confocal microscopic images with *z*-clipping along *x* and *y* axes were not checked since no additional useful information can be provided in these two cases.

[36] For the glucose analog, see: T. Buskas, E. Soederberg, P. Konradsson, B. Fraser-Reid, *J. Org. Chem.* **2000**, *65*, 958.